Distinct local electronic structure and magnetism for Mn in amorphous Si and Ge

Li Zeng (曾立),[1,*] J. X. Cao,[2] E. Helgren,[1] J. Karel,[3] E. Arenholz,[4] Lu Ouyang,[5] David J. Smith,[5] R. Q. Wu,[2] and F. Hellman[1,†]

[1]*Department of Physics, University of California, Berkeley, California 94720, USA*
[2]*Department of Physics and Astronomy, University of California, Irvine, California 92697, USA*
[3]*Department of Materials Science and Engineering, University of California, Berkeley, California 94720, USA*
[4]*Advanced Light Source, Lawrence Berkeley National Laboratory, Berkeley, California 94720, USA*
[5]*Department of Physics, Arizona State University, Tempe, Arizona 85287, USA*

(Received 15 April 2010; published 14 October 2010)

Transition metals such as Mn generally have large local moments in covalent semiconductors due to their partially filled *d* shells. However, Mn magnetization in group-IV semiconductors is more complicated than often recognized. Here we report a striking crossover from a quenched Mn moment ($<0.1\mu_B$) in amorphous Si (*a*-Si) to a large distinct local Mn moment ($\geq 3\mu_B$) in amorphous Ge (*a*-Ge) over a wide range of Mn concentrations (0.005–0.20). Corresponding differences are observed in *d*-shell electronic structure and the sign of the Hall effect. Density-functional-theory calculations show distinct local structures, consistent with different atomic density measured for *a*-Si and *a*-Ge, respectively, and the Mn coordination number N_c is found to be the key factor. Despite the amorphous structure, Mn in *a*-Si is in a relatively well-defined high coordination interstitial type site with broadened *d* bands, low moment, and electron (*n*-type) carriers, while Mn in *a*-Ge is in a low coordination substitutional type site with large local moment and holes (*p*-type) carriers. Moreover, the correlation between N_c and the magnitude of the local moment is essentially independent of the matrix; the local Mn moments approach zero when $N_c > 7$ for both *a*-Si and *a*-Ge.

DOI: 10.1103/PhysRevB.82.165202 PACS number(s): 75.50.Pp, 75.20.Hr, 71.23.Cq, 75.50.Kj

I. INTRODUCTION

At the advent of the contemporary semiconductor era, transition metals (TMs) were viewed as undesirable impurities in group-IV semiconductors. Ludwig and Woodbury developed a model which successfully explained the electronic structure of TM impurities in crystalline Si (*c*-Si).[1] It is well established that $\sim 10^{16}/\mathrm{cm}^3$ TM impurities create enough deep level states to significantly trap charge carriers and hinder transport.[2] More recently, exploration of novel ways to manipulate electron spins has made TM dopants of interest in diluted magnetic semiconductors (DMSs) for spintronic applications, where both charge and spin are manipulated and utilized for information processing.[3–8] Magnetic semiconductors based on group-IV materials, such as Si or Ge, are especially interesting due to their predicted high critical temperature T_c and predominance as mainstream semiconductor materials for microelectronics. In the model DMS system (Ga,Mn)As, it is found that various Mn doping sites have different local moments, critical to the magnetic properties.[9–11] However, similar studies of Mn in Si and Ge are missing due to the much less controlled doping environment and extremely low solubility, and achieving intrinsic ferromagnetism at ambient conditions in Si/Ge is challenging. Although first-principles calculations suggest a local Mn moment for both interstitial and substitutional doping sites, and a high T_c in *p*-type Si or Ge,[12–14] experimental results reported in the literature, such as T_c and saturation moment, are very diverse even for samples prepared using similar methods. High T_c (up to 400 K) were reported for Mn doped in *c*-Si (Ref. 15) and *c*-Ge,[14,16,17] but these samples were inhomogeneous, containing clusters,[15,18] nanocrystallites,[19,20] nanocolumns,[16] or chemical inhomogeneity.[17] It is therefore difficult to know or understand the intrinsic magnetic properties.

To overcome this issue, we have worked instead with an *amorphous* Si (*a*-Si) or Ge (*a*-Ge) matrix. For group-IV semiconductors, the amorphous structure preserves local tetrahedral fourfold covalent bonding, described by the continuous random network model.[21–24] Even when doped up to 20–25 at. % with atoms such as Nb, Y, or the large magnetic rare-earth ion Gd, *a*-Si and *a*-Ge remain chemically homogeneous and amorphous, as measured by high-resolution transmission electron microscopy, extended x-ray-absorption fine structure, energy dispersive x-ray (EDX), and other chemical and structural analysis tools.[25–27] While in some respects, the electronic and optical properties of amorphous metal semiconductor alloys and doped crystalline semiconductors are quite different, there are also profound similarities, perhaps most strikingly in the temperature, frequency, and composition scaling properties near the insulator-metal (*I-M*) transition in each.[28,29] The loss of translational symmetry creates band tails and changes the nature of the band gap but does not alter the underlying semiconducting nature (e.g., an absorption edge is still seen optically, but the distinction between indirect and direct gap is lost). The amorphous structure introduces strong scattering and deep electrical traps due to disorder; yet both systems are insulating at low dopant concentrations and exhibit a concentration-tuned *I-M* transition at higher dopant concentration. The strong disorder makes the dopant concentration (e.g., of Nb in *a*-$\mathrm{Nb}_x\mathrm{Si}_{1-x}$) at which the transition occurs be orders of magnitude larger than in the crystalline counterpart (e.g., P in crystalline Si:P) but at low temperature, the temperature, frequency, and concentration dependence of electrical conductivity are the same for these two systems.[29,30] Fur-

thermore, the accommodating nature of the amorphous systems has allowed some studies to be made which have either no or limited counterparts in crystalline systems. For example, the magnetic moment of Gd allowed detailed studies (optical, magneto-optical, magnetotransport, and tunneling spectroscopy) of a magnetic field-tuned *I-M* transition in a-Gd_xSi_{1-x}; these materials show enormous negative magnetoresistance (MR) at low temperatures, an indication of strong moment-carrier interactions and spin polarized carriers.[31,32] A somewhat analogous study has been done on the crystalline compound Gd-S,[33] but there is no counterpart in crystalline doped Si due to the issues of inhomogeneity discussed above. Ferromagnetism is robust to disorder, and the localized Mn d moment should depend only on local environment, which for group-IV semiconductors is similar in crystalline and amorphous structures. Thus, there is no fundamental reason that the matrix must be crystalline to have ferromagnetic states and spin polarized carriers, although high mobility conductivity would be precluded.[34–36] The great advantage to amorphous magnetic semiconductors is low growth temperature and metastability of a homogeneous phase, inhibiting insolubility and phase separation issues inherent in the crystalline systems.

Here, we report unexpected and radically different magnetic and electronic properties of Mn-doped a-Si and a-Ge (a-Mn_xSi_{1-x} and a-Mn_xGe_{1-x}). For x ranging from 0.005 to 0.20, all samples are found to be homogeneous and amorphous despite Mn doping well above the solid solubility limit for crystalline Si and Ge. We observe striking dissimilarities in magnetic properties: while a large Mn moment is observed in a-Ge, it is totally quenched (nonmagnetic) in a-Si, leading to fundamentally different magnetic ground states and magnetotransport properties. These two "similar" systems have opposite signs of carriers and MR, and very different x-ray absorption spectra and concentration dependence of the atomic density. The quenched Mn moment was first observed and reported in our earlier work[37] and x-ray absorption spectroscopy (XAS) at Mn L edges suggested itinerant d states with no multiplet features.[38] However, the underlying mechanism and microscopic origin for this effect was unclear. In this paper, through a systematic study of the matrix dependence of magnetization, we show a crossover for Mn from itinerant band states to localized magnetic moments, which is exquisitely sensitive to the local coordination number around Mn dopants.

II. EXPERIMENTAL METHOD

Mn-doped a-Si and a-Ge films were prepared by e-beam coevaporation under ultrahigh-vacuum conditions (base pressure below 10^{-9} Torr) onto 400 nm amorphous SiN_x-coated Si substrates held near room temperature. Thickness monitors for individual sources ensured independent real-time flux control in order to achieve homogeneous doping profiles. Growth rates of ~ 2 Å/s were used. High-resolution cross-sectional transmission electron micrographs (HR-XTEM) and EDX analysis were performed to check sample crystallinity and homogeneity. Film compositions and absence of measurable oxidation were determined by Rutherford backscattering (RBS) with O resonance energy (incident energy of ~ 4 MeV). No oxygen was detected in the bulk of the films when films were protected from exposure to air by capping layers of Si, Al, or Au, depending on the measurement to be made (surface oxygen *was* found when samples were not protected). XAS and x-ray magnetic circular dichroism (XMCD) spectra at the Mn L edges were recorded at the Advanced Light Source beam line 6.3.1 in total electron yield mode. All samples for XAS and XMCD, including a control sample of pure Mn metal film, were capped with 2–4 nm of Al or Au and stored in a vacuum desiccator to avoid oxidation. Commercially available Mn oxide powders with different Mn valences (MnO, Mn_2O_3, and MnO_2, corresponding to d^5, d^4, and d^3 configurations, respectively) were used as references.

Magnetization was measured using a commercial superconducting quantum interference device magnetometer (MPMS system, Quantum Design). Bare substrates from the same batch were measured at the same temperature and field values (the signal is purely diamagnetic as expected) and subtracted point-by-point for all magnetization analysis. dc transport and magnetotransport measurements were performed using a standard four point probe technique. Samples were made with different thicknesses (150 and 400 nm for a-Mn-Si, 150, 200, and 250 nm for a-Mn-Ge) to test for thickness dependence (none was found).

Density-functional-theory (DFT) calculations were performed using a unit cell of 64 atoms. The amorphous structure was obtained by quenching and annealing N_{Mn} Mn atoms and $(64-N_{Mn})$ Si or Ge atoms. The *ab initio* molecular-dynamics (MD) functionality was implemented in the Vienna *ab initio* simulation package (VASP). Projector augmented wave pseudopotentials were used for the electron-ion interaction. Density-functional Kohn-Sham equations were solved at the level of generalized gradient approximation with the PW91 functional, and the GGA+U approach was also used to examine the correlation effect for some cases. The energy cutoff for the expansion of wave function was 350 eV. While only the Γ point was used to sample the Brillouin zone during the quench and annealing process, $3\times3\times3$ Monkhorst-Pack k points and $6\times6\times6$ Monkhorst-Pack K points were used for geometry relaxations and determination of electronic and magnetic properties, respectively. For the initial structure, Mn atoms were randomly substituted for Si or Ge. The lattice sizes were optimized ahead of the MD simulations (fixed $a=b=c$). To obtain reliable statistics, 20 independent initial configurations were used for each concentration in a-Mn_xGe_{1-x} and a-Mn_xSi_{1-x}. Results of mass density, pair correlation function, and density of states for pure a-Si agreed well with previous studies that used much larger unit cells.[39,40] For example, mass density for optimized a-Si was 2.27 g/cm^3, a value that agrees well with experimental data.

III. EXPERIMENTAL RESULTS

We start with comparison of transport properties. Figure 1 shows $\sigma_{dc}(T)$ for a-Mn_xSi_{1-x} and a-Mn_xGe_{1-x}; the data for each show a clear monotonic increase with x, confirming the

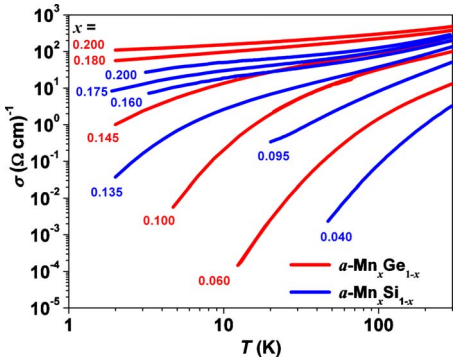

FIG. 1. (Color online) Temperature dependence of dc conductivity $\sigma(T)$ for a-Mn_xSi_{1-x} and a-Mn_xGe_{1-x} for various concentrations x across the I-M transition. As x increases for each, the magnitude of $\sigma(T)$ increases monotonically and an I-M quantum phase transition is seen in both sets of samples, with critical concentrations $x_c \sim 0.14$ found by fits to low T data. σ increases with T, a result of localization and Coulomb effects in disordered electronic systems.

efficacy of Mn as a dopant in both matrices. Like doped crystalline semiconductors, an I-M transition is seen as a function of doping concentration x in both a-Mn_xSi_{1-x} and a-Mn_xGe_{1-x}. The positive $d\sigma/dT$ for all samples is a signature of a strongly disordered electronic system near the I-M transition.[28] For this three-dimensional quantum phase transition, the observed I-M transition is rigorously defined by the ground state dc conductivity σ_{dc} at $T=0$. $\sigma_{dc}(T)$ as $T \rightarrow 0$ vanishes for insulators in an exponential form, while for metals it remains nonzero as $T \rightarrow 0$.[28] The critical concentration x_C for the I-M transition is ~ 0.14 in both a-Mn_xSi_{1-x} and a-Mn_xGe_{1-x}, similar to other amorphous metal-doped semiconductors.[23,26] (x_C is enhanced by orders of magnitude compared to crystalline counterparts such as c-Si:P due in part to strong charge carrier localization in the amorphous structure, and in part to differences in the depth of the dopant energy levels[41]) For a given x, a-Mn_xGe_{1-x} has higher $\sigma_{dc}(T)$ than a-Mn_xSi_{1-x}, presumably because of the smaller band gap of Ge. Hall measurements were performed on metallic samples of each. Due to large carrier concentrations ($\sim 10^{22}/\mathrm{cm}^3$) and longitudinal MR (positive for a-Mn_xSi_{1-x}, negative for a-Mn_xGe_{1-x}), carrier information was found from the asymmetry in the transverse resistivity $\Delta\rho_{xy}(H) = \rho_{xy}(+H) - \rho_{xy}(-H)$. $\Delta\rho_{xy}(H)$ is linear for both; the sign of the slope indicates electronlike and holelike charge carriers in a-Mn_xSi_{1-x} and a-Mn_xGe_{1-x}, respectively.

Figure 2(a) shows dc magnetic susceptibility $\chi(T)$ measured in 100 Oe field for typical a-Mn_xSi_{1-x} and a-Mn_xGe_{1-x} samples with similar x. The differences are striking: a-Mn_xGe_{1-x} has much larger $\chi(T)$, with a distinct cusp at a temperature T_f (~ 9 K for $x=0.15$) in the zero-field-cooled

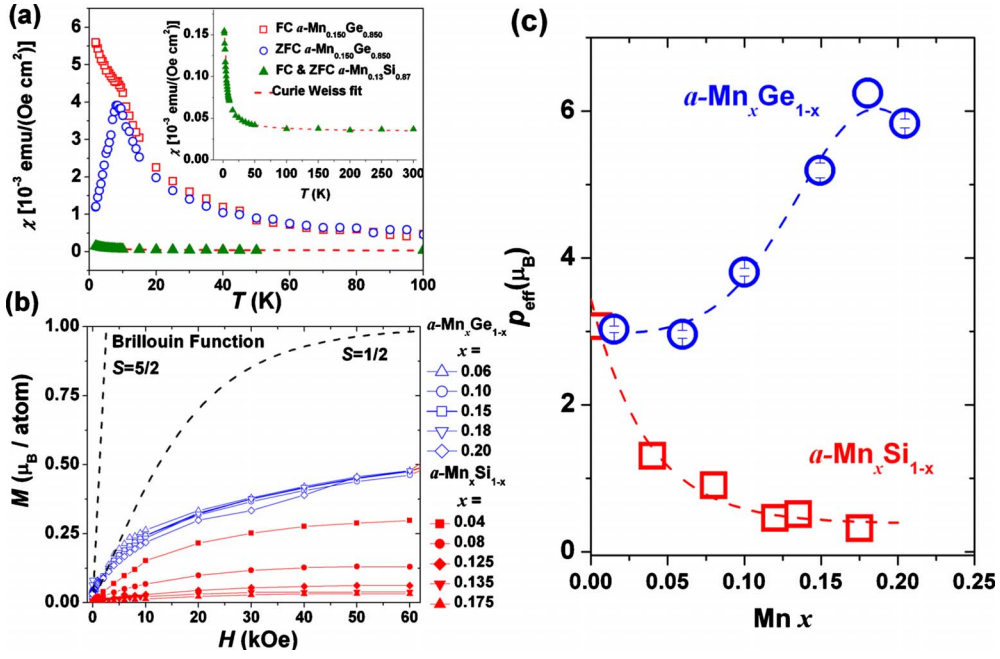

FIG. 2. (Color online) Magnetic properties of a-Mn_xSi_{1-x} and a-Mn_xGe_{1-x}. (a) zero-field-cooled and field-cooled magnetic susceptibility $\chi(T)$ data for typical samples. For a-Mn_xSi_{1-x} (green solid triangles), $\chi(T)$ is negligible compared to $\chi(T)$ of a-Mn_xGe_{1-x} (blue and red open circles and squares). Inset shows the same a-Mn_xSi_{1-x} data on expanded scale. The red dashed line is a Curie fit. (b) M vs H data measured at $T=2$ K normalized to the number of Mn atoms. The dashed lines are BFs for $J=S=5/2$ and 1/2 and $g=2$ (pure spin state). For a-Mn_xGe_{1-x} (blue open symbols), all $M(H)$ data collapse, are suppressed well below either BF and show no sign of saturation to $H=6$ kOe. For a-Mn_xSi_{1-x} (red solid symbols), $M(H)$ data behave like free moments but with very small saturation moments (values dependent on x and less than $0.3\mu_B$). (c) Concentration dependence of effective moment p_{eff} of a-Mn_xGe_{1-x} (blue circles) and a-Mn_xSi_{1-x} (red squares), calculated from $\chi(T)$ data (above T_f for a-Mn_xGe_{1-x}) assuming all Mn are magnetically active. p_{eff} of a-Mn_xSi_{1-x} vanishes, distinct from the large p_{eff} of a-Mn_xGe_{1-x}, which shows an increase with x. For a-Mn_xSi_{1-x}, a better and consistent fit for $\chi(T)$ and $M(H,T)$ is obtained by assuming S=5/2 for a tiny fraction of noninteracting Mn ($\sim 10^{-3}$). For a-Mn_xGe_{1-x}, the distinct local moments interact with strongly mixed AFM and FM interactions, suppressing $M(H,T)$ far below the BF.

(ZFC) data. Field-cooled (FC) $\chi(T)$ is split from ZFC data below T_f. This suggests a spin-glass ground state for a-Mn_xGe_{1-x}, similar to Gd-doped ($J=S=7/2$) a-Si and a-Ge, resulting from competing ferromagnetic (FM) and antiferromagnetic (AFM) interactions.[23,42] Above T_f, $\chi(T)$ is well fit by a Curie-Weiss law with large effective moment near that for $S=3/2-5/2$. By contrast, a-Mn_xSi_{1-x} has very small $\chi(T)$, fit well with a simple Curie law with low effective moment, and shows no sign of spin-glass freezing (down to 1.9 K, the lowest measured T).

Figure 2(b) shows the field-dependence of magnetization per Mn atom $[M(H)]$ for all a-Mn_xSi_{1-x} and a-Mn_xGe_{1-x} samples at $T=2$ K, assuming all Mn atoms are equally magnetically active (this assumption is not likely true for a-Mn_xSi_{1-x} as will be explained later). There are a number of remarkable features to note. First, $M(H)$ is well below the Brillouin functions (BFs) for either $S=5/2$ or 1/2 for both a-Si and a-Ge matrices but, like $\chi(T)$, is significantly smaller for a-Mn_xSi_{1-x}, particularly for higher x, and with completely different dependence on x. Second, for a-Mn_xSi_{1-x}, dM/dH approaches 0 at high H, which is a sign of saturation, despite being well below the expected BF. Third, for a-Mn_xGe_{1-x} the small moment and significant slope dM/dH at high field despite the large $\chi(T)$ can only be interpreted as due to strong frustrated magnetic interactions, consistent with the spin-glass freezing seen in $\chi(T)$.[43] The collapse of a-Mn_xGe_{1-x} $M(H)$ data, independent of x, indicates a similarity of Mn moments and interactions, similar to what was seen in a-Gd_xSi_{1-x} and a-Tb_xSi_{1-x}.[44]

The difference between the two systems is best seen in the x dependence of effective moment p_{eff}, shown in Fig. 2(c). p_{eff} is obtained by fitting $\chi(T)$ to a Curie-Weiss (CW) form: $\chi(T)=A/(T-\theta)+b$ ($T>T_f$ for a-Mn_xGe_{1-x}), with CW fitting constant $A=N_{Mn}p_{eff}^2\mu_B^2/3k_B$, b=diamagnetic background constant, and N_{Mn}=number density of Mn atoms (determined by RBS and film area). For a-Mn_xGe_{1-x}, p_{eff} is $\geq 3\mu_B$, increasing with x to $\sim 6\mu_B$. In contrast, p_{eff} of a-Mn_xSi_{1-x} monotonically *decreases* and is negligible (less than $0.1\mu_B$) at higher x. This small p_{eff} is consistent with the low saturation moment seen in Fig. 2(b). A consistent fit of *all* a-Mn_xSi_{1-x} magnetic data is obtained by assuming an $S=5/2$ paramagnetic state, with a tiny fraction ($\sim 10^{-3}$) of Mn being magnetically active and the majority of Mn d moments quenched.[38] The (small) positive MR seen at 2 K in a-Mn_xSi_{1-x} is thus simply explained—there are no moments and hence no significant moment-carrier interactions to produce negative MR, so MR is similar to that seen in other nonmagnetic doped semiconductors. The negative MR in a-Mn_xGe_{1-x} is due to the same moment-carrier interactions and I-M physics as a-Gd_xSi_{1-x}; it is small (relative to a-Gd_xSi_{1-x}) because of increased AFM Mn-Mn interactions, reflected in the very low $M(H)$ shown in Fig. 2(b).

XAS at the Mn $L_{2,3}$ edges provides direct information about the d shell electronic structure that determines magnetism. Figure 3 shows XAS data for a-Mn_xGe_{1-x} and a-Mn_xSi_{1-x}, as well as results from Mn metal and Mn oxides for reference. a-Mn_xSi_{1-x} shows two broad smooth absorption peaks with no atomic multiplet features, suggesting that the quenched Mn moment in a-Si is due to itinerant d states existing even in a very insulating sample ($x\sim 0.005$).[38] The

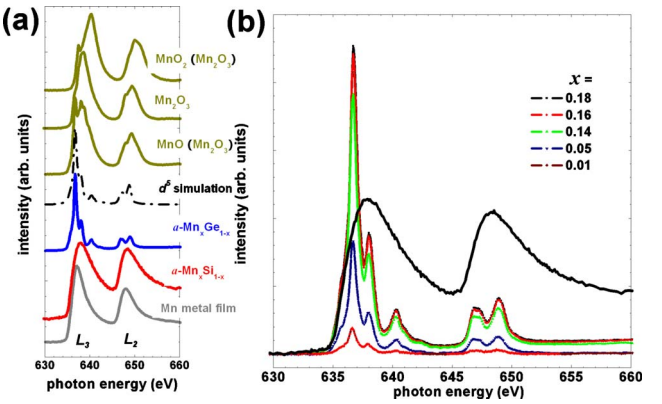

FIG. 3. (Color online) X-ray absorption spectroscopy of Mn L edges in different materials. $L_{3,2}$ edges measure the transition from occupied p states to unoccupied d states. (a) Mn L edges of a-Mn_xGe_{1-x} resembles the spectra of Mn oxides, which show atomic multiplet features associated with localized d electronic states. The dash-dotted line is a simulated spectrum for $3d^5$. On the other hand, Mn in a-Mn_xSi_{1-x} resembles Mn metal films with smooth and broad L edges without any multiplet feature but is different from Mn metal films in peak positions and peak width. (b) L edges of a-Mn_xGe_{1-x} for different x show the same multiplet lineshape. When normalized by the postedge jump intensity, all a-Mn_xGe_{1-x} XA spectra collapse to the same curve. A typical XA spectrum of a-Mn_xSi_{1-x} (with two broad peaks) is also plotted here to show the difference in line shape. Due to different capping layer and surface sensitivity, a-Mn_xSi_{1-x} does not scale well with postedge jump intensity for small x.

results are quite different for a-Mn_xGe_{1-x}, which shows a distinct multiplet line shape for all x. The absorption intensity of these data scales with x, with all a-Mn_xGe_{1-x} curves collapsing to a single line shape similar to XAS reported for substitutional Mn in c-Ge.[45,46] XMCD measurements were also performed on all XAS samples (both for a-Mn_xGe_{1-x} and a-Mn_xSi_{1-x} for multiple concentrations listed in Fig. 3). There is no XMCD signal from all these samples down to the lowest measured temperature (8 K) and the highest measured field (21 kOe), consistent with the small magnetization shown in $M(H)$ results. For a-Mn_xSi_{1-x}, the moment is quenched, and the small paramagnetic portion would not give an XMCD signal at our measurement conditions. In a-Mn_xGe_{1-x}, though there is a large local moment, the Mn interactions are strongly frustrated due to the developing spin-glass phase at low temperatures, again leading to an XMCD signal below measurement threshold.

Figures 4(a) and 4(b) show HR-XTEM micrographs for two typical samples of a-$Mn_{0.15}Si_{0.85}$ and a-$Mn_{0.19}Ge_{0.81}$. EDX scans were also performed to look for chemical inhomogeneity. No crystallinity or inhomogeneity was seen for any a-Mn_xSi_{1-x} or a-Mn_xGe_{1-x} ($x<0.20$). A very few places (diameters <2 nm) displayed suggestions of poorly defined lattice fringes, but digital diffractograms confirmed typical amorphous structure. These micrographs show no second phase or nanocrystallite formation commonly observed in crystalline films.[15–17,19,20] a-Mn_xSi_{1-x} and a-Mn_xGe_{1-x} samples are thus homogeneous and uniform to the microscope resolution limit of 0.17 nm, and differences

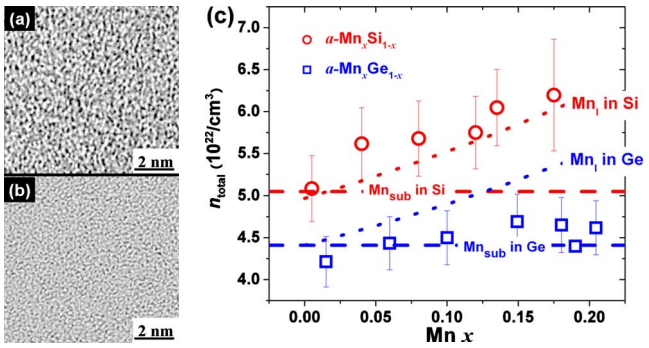

FIG. 4. (Color online) Structural analysis of a-Mn_xSi_{1-x} and a-Mn_xGe_{1-x}. (a) and (b) High-resolution cross-sectional transmission electron micrographs for a-$Mn_{0.15}Si_{0.85}$ and a-$Mn_{0.19}Ge_{0.81}$ samples showing an amorphous structure with no indication of any second phase or clustering. (c) Total atomic number density as a function of concentration x. Symbols are data from RBS and thickness measurements (red and blue for a-Mn_xSi_{1-x} and a-Mn_xGe_{1-x}, respectively). The red and blue dotted (dashed) lines are number densities calculated for interstitial (substitutional) Mn in Si and Ge, respectively. For a-Mn_xSi_{1-x} samples, there is a strong concentration dependence matching closely the expectation for interstitial Mn in Si (with a constant n_{Si}), while for a-Mn_xGe_{1-x}, there is no concentration dependence, suggesting substitutional Mn in Ge.

in magnetization do not arise from microstructural inhomogeneity.

The total number density n (atoms/cm^3) was determined by measuring areal density N_A (atoms/cm^2) by RBS and film thickness t by atomic force microscopy ($n=N_A/t$); results are shown in Fig. 4(c). High-quality pure a-Si and a-Ge films have n very close to their crystalline forms (~98%) because they preserve short-range tetrahedral ordering and have low vacancy concentrations.[21,47] Fig. 4(c) shows that $n(x)$ for a-Mn_xSi_{1-x} and a-Mn_xGe_{1-x} have the expected density at low x but very different x dependence as x increases. $n(x)$ for a-Mn_xSi_{1-x} monotonically increases, while $n(x)$ for a-Mn_xGe_{1-x} has almost no x dependence. If Mn dopants occupy interstitial-like sites, with no change in lattice spacing, $n(x)$ should increase with x, whereas $n(x)$ should be independent of x for the substitutional-like case. The data suggest that Mn atoms in a-Si are in an interstitial-like environment, while Mn atoms in a-Ge are in a substitutional-like environment, consistent with what has been suggested for crystalline counterparts at very low x.

Mn at interstitial-like sites would have more Si neighbors hence possibly stronger p-d hybridization, causing the d band to lose its localized nature, similar to what occurs in weak itinerant metallic FM Mn silicides ($MnSi_{1.7}$), in which M is tiny.[48] On the other hand, substitutional Mn in Ge is predicted to have a local moment of $\sim 3\mu_B$,[12,14] as was measured for the low x a-$Mn_{0.01}Ge_{0.99}$, and to act as a double acceptor, consistent with our Hall effect data. It is not clear why M per Mn increases with x in a-Ge, but the collapse of XAS data shows that this is not due to changes in $3d$ shell occupation of Mn. It may be due to polarization of holelike carriers.

Experimental results from various measurements (transport, magnetic, and structural analyses) thus paint a consistent picture that explains the difference in magnetism between a-Mn_xSi_{1-x} and a-Mn_xGe_{1-x}, two deceptively similar systems. We conclude that Mn occupies interstitial-like sites in a-Mn_xSi_{1-x} but substitutional-like sites in a-Mn_xGe_{1-x}. Over the wide Mn doping range studied ($x=0.005-0.2$), the monotonic x dependencies of $\sigma(T)$, $\chi(T)$, and XAS intensity, as well as the x-independent $M(H)$ and XAS line shape, all show that Mn is uniformly incorporated in each matrix. The qualitative differences in magnetization and associated differences in MR originate from different local atomic environments of Mn in each matrix.

IV. DFT CALCULATION RESULTS

To better understand and test this proposed model, first-principles calculations were carried out. The ability to interrogate local parameters in the simulated structure provides a powerful tool to probe correlations between local moment and local structure. Structural and electronic properties including local moments were calculated for three Mn concentrations, $x=0.016$, 0.094, and 0.156 (corresponding to $N_{Mn}=1$, 6, and 10 in a 64-atom supercell) for a-Si and a-Ge using *ab initio* molecular dynamics and solving the Kohn-Sham equations with the generalized gradient approximation. The amorphous structures were obtained by creating a supercell containing N_{Mn} Mn atoms plus $(64-N_{Mn})$ Si or Ge atoms randomly substituted on zinc-blende crystal structure sites. This initial configuration was first "melted" at ~1800 K, then quenched at a rate of 2.4×10^{14} K/s to 600 K, then annealed for 10 ps at 600 K in the constant temperature $[NV(T)]$ ensemble and finally quenched and relaxed to 0 K. The final configurations were further relaxed with an atomic force criterion that requires the calculated maximum force amplitude to be smaller than 0.01 eV/Å. Similar procedures have been extensively applied in studies of amorphous silicon.[39,40,49] To obtain reliable statistics, 20 independent initial configurations were used for each concentration. More details regarding calculations can be found in Sec. II. For each concentration, the average magnetic moment M was calculated according to the statistics for canonical ensembles as $M=(1/N_{Mn})\Sigma_{n=1}^{N} m_n \exp(E_n/k_BT)/\Sigma_{n=1}^{N}\exp(E_n/k_BT)$, where $N=20$ is the number of configurations, and E_n and m_n are the total energy and magnetic moment for each final configuration. We find that M increases with x for a-Mn_xGe_{1-x} but decreases with x for a-Mn_xSi_{1-x} to a very small value ($0.043\mu_B$ for $x=0.156$), reproducing well the experimental data shown in Fig. 2.

To identify the origin of the vanishing magnetization in a-Mn_xSi_{1-x}, whether it stems from decrease in the local moment or cancellation through AFM coupling, we calculate and show in Fig. 5 the magnetic moment distribution function $\rho(m)=(1/N\times N_{Mn})\Sigma_{n=1}^{N}\Sigma_{j=1}^{N_{Mn}} g(m-m_n^j)$, where m_n^j is the magnetic moment of the jth Mn atom in the nth final configuration and δ functions are represented by normalized Gaussian functions $g(z)$. $\rho(m)$ for a-Mn_xSi_{1-x} is predominantly at $m=0\mu_B$, indicating zero local moment for the majority of Mn atoms in a-Si. Thus, the dramatic quench of magnetization in a-Mn_xSi_{1-x} is because of vanishing local

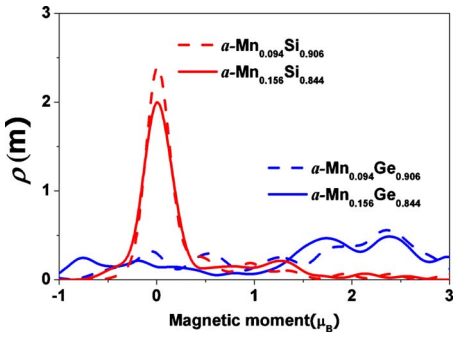

FIG. 5. (Color online) DFT results for magnetic moment distribution $\rho(m)$. For a-Mn_xSi_{1-x}, $\rho(m)$ is centered at zero moment; thus the lack of magnetization is due to lack of local moments instead of any AFM coupling. For a-Mn_xGe_{1-x}, significant moment distribution is between $1.5-3.0\mu_B$ with almost no distribution at low moment. Data are not shown for the lowest concentration $x=0.0156$ due to poor statistics (only 20 data points from one Mn atom in each 20 configurations)

moment. By contrast, the most probable values of m in a-Mn_xGe_{1-x} are in the range of $1.5-3.0\mu_B$. Varying the supercell size (still with 64 atoms) from 10.95–11.54 Å (corresponding to mass densities 2.27–1.94 g/cm^3 for a-Si), which causes changes of interatomic spacing, was found to have only a small influence on M or $\rho(m)$ (less than $0.1\mu_B$). Replacing Si by Ge without altering the structure also does not change M or $\rho(m)$. It is therefore clear that the lack of moment in a-Mn_xSi_{1-x} is not due to differences in Mn-Si/Mn-Ge distances or bonding chemistry but lies instead in the different atomic arrangements of the two structures, which we next discuss.

Figure 6(a) shows pair correlation functions (PCFs) for Mn-Si and Mn-Ge for $x=0.094$. The first peak locations, corresponding to the most probable nearest bond length, are slightly different due to the difference in Si and Ge atomic size. However, the quite different first peak *heights* show that Mn in Si has a significantly larger coordination number N_c (more Si nearest neighbors) than Mn in Ge. We define the coordination number N_c in these amorphous samples using the first minimum in the PCF as a cutoff distance. The inset shows Si-Si and Ge-Ge PCFs for the same concentration; these agree with typical values for a-Si and a-Ge, showing that the matrices are largely unaffected by Mn doping. Figure 6(b) shows the statistics for all Mn atoms in the 20 final configurations, indicating that Mn atoms mostly have five or six nearest neighbors in a-Ge but seven or eight nearest neighbors in a-Si. Figure 6(c) shows the local moment as a function of N_c. There is a strong correlation between N_c and the magnitude of the moment, essentially independent of whether the matrix is Si or Ge:Mn becomes nonmagnetic for $N_c \geq 7$. Calculations with the GGA+U ($U=4.0$ eV) confirmed that the inclusion of electron-correlation effect at Mn sites does not affect these results.

Finally, Fig. 6(d) plots the spin up and spin down locally projected density of states (PDOS) for three Mn atoms in a-$Mn_{0.094}Ge_{0.906}$ with different N_c. There is a large imbalance in PDOSs for the two occupied spin channels when $N_c=5$ or 6, which leads to a net moment for the majority of Mn in a-Ge. The imbalance decreases with N_c, and approaches zero when $N_c=8$, which is a rare configuration for a-Mn_xGe_{1-x} but the predominant configuration for a-Mn_xSi_{1-x}. Different N_c is thus the key parameter that leads to dramatically different magnetization for a-Mn_xSi_{1-x} and a-Mn_xGe_{1-x}. We also found that the number of electrons in Mn atoms increases with N_c,[48] suggesting that Mn atoms with $N_c=7-8$ provide electrons but those with $N_c=4-5$ provide holes, in good accord with behavior of Mn dopants at interstitial and substitutional sites, respectively. Furthermore, we found that Mn prefers geometries with $N_c=4-6$ in a-Ge, almost regardless of concentration. In contrast, for a-Si with $x=0.094$ and 0.156 most Mn atoms have $N_c=6-8$, while at very low x, where the Mn-induced lattice distortion is rather limited, smaller N_c is found. It is known that Mn prefers substitutional sites in crystalline Ge and interstitial sites in crystalline Si because of the smaller size of Si and higher energy cost to break Si-Si bonds.[39,49] It appears that this difference

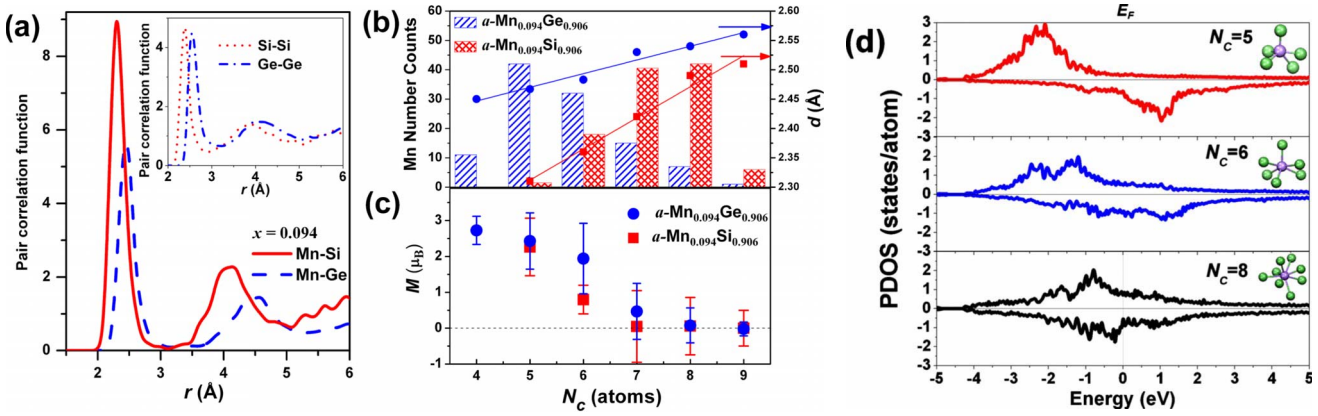

FIG. 6. (Color online) Pair correlation functions (PCFs), locally projected density of states (PDOS) on Mn, and statistics of local parameters as a function of the number of nearest neighbors for Mn concentration $x=0.094$. (a) Mn-Si (red solid line) and Mn-Ge (blue dashed line) PCFs. Inset: Si-Si (red dotted line) and Ge-Ge (blue dash-dotted line) PCFs. (b) Statistical counts of the 120 Mn atoms in all 20 configurations (red and blue bars for Si and Ge, respectively) and the average Mn-Si (red squares) and Mn-Ge distances (blue circles) d as a function of the number of Si or Ge nearest neighbors N_c. (c) Local Mn moment M in each matrix vs N_c. (d) PDOS for majority and minority spins of three Mn atoms with different N_c in a-$Mn_{0.094}Ge_{0.906}$.

is still present and leads to more fundamental difference in amorphous structures.

V. CONCLUSIONS

In summary, Mn doping in amorphous group-IV semiconductors exhibits two distinct behaviors: the complete quenching of the Mn moment in Si and its preservation in Ge is directly linked to coordination number N_c. Even though this is deduced from the amorphous structure, N_c as a universal local parameter should apply to Mn d electrons in crystalline samples, at interfaces of heterostructures or in self-assembly nanostructure or clusters. Some recent theoretical calculations based on MnSi compound[50] and Mn at the Si surface[51] have also suggested the potential influence of N_c; we here unambiguously correlate N_c with local Mn moment. Our discovery of a quenched moment for high-N_c sites accounts for some of the mysterious "magnetically silent" dopants and explain the great variation of moment/Mn values in the literature. Control of the local environment, and specifically the need to have Mn in low coordination sites, is thus critical to a robust Mn moment and to making magnetic semiconductors. Moreover, these results, showing a crossover from localized to itinerant moments of a d-band element in a covalently bonded semiconductor matrix, represent a significant example of high moment/low moment crossovers in d-band magnetism in solids.

ACKNOWLEDGMENTS

Synthesis and most measurements were supported by NSF Grant No. DMR-0505524. Characterization and work at the Advanced Light Source were supported by DOE Office of Basic Energy Sciences under Contract No. DE-AC02-05CH11231. Work at UCI was supported by DOE Office of Basic Energy Sciences under Contract No. DE-FG02-05ER46237. Calculations were performed on parallel computers at NERSC. We acknowledge use of facilities in the John M. Cowley Center for High Resolution Electron Microscopy at Arizona State University.

*Present address: NSF Nano-Scale Science and Engineering Center (NSEC), 3112 Etcheverry Hall, University of California, Berkeley, California 94720, USA.
†fhellman@berkeley.edu

[1] G. W. Ludwig and H. H. Woodbury, Phys. Rev. Lett. **5**, 98 (1960).
[2] E. R. Weber, Appl. Phys. A: Mater. Sci. Process. **30**, 1 (1983).
[3] S. A. Wolf, D. D. Awschalom, R. A. Buhrman, J. M. Daughton, S. von Molnar, M. L. Roukes, A. Y. Chtchelkanova, and D. M. Treger, Science **294**, 1488 (2001).
[4] H. Munekata, H. Ohno, S. von Molnar, A. Segmüller, L. L. Chang, and L. Esaki, Phys. Rev. Lett. **63**, 1849 (1989).
[5] H. Ohno, A. Shen, F. Matsukura, A. Oiwa, A. Endo, S. Katsumoto, and Y. Iye, Appl. Phys. Lett. **69**, 363 (1996).
[6] J. Fabian, A. Matos-Abiague, C. Ertler, P. Stano, and I. Zutic, Acta Phys. Slov. **57**, 565 (2007).
[7] H.-J. Jang and I. Appelbaum, Phys. Rev. Lett. **103**, 117202 (2009).
[8] B. Huang, D. J. Monsma, and I. Appelbaum, Phys. Rev. Lett. **99**, 177209 (2007).
[9] K. M. Yu, W. Walukiewicz, T. Wojtowicz, I. Kuryliszyn, X. Liu, Y. Sasaki, and J. K. Furdyna, Phys. Rev. B **65**, 201303(R) (2002).
[10] K. M. Yu, W. Walukiewicz, T. Wojtowicz, W. L. Lim, X. Liu, U. Bindley, M. Dobrowolska, and J. K. Furdyna, Phys. Rev. B **68**, 041308(R) (2003).
[11] M. A. Scarpulla, O. D. Dubon, K. M. Yu, O. Monteiro, M. R. Pillai, M. J. Aziz, and M. C. Ridgway, Appl. Phys. Lett. **82**, 1251 (2003).
[12] A. P. Stroppa, S. Picozzi, A. Continenza, and A. J. Freeman, Phys. Rev. B **68**, 155203 (2003).
[13] Y.-J. Zhao, T. Shishidou, and A. J. Freeman, Phys. Rev. Lett. **90**, 047204 (2003).
[14] Y. D. Park, A. T. Hanbicki, S. C. Erwin, C. S. Hellberg, J. M. Sullivan, J. E. Mattson, T. F. Ambrose, A. Wilson, G. Spanos, and B. T. Jonker, Science **295**, 651 (2002).
[15] M. Bolduc, C. Awo-Affouda, A. Stollenwerk, M. B. Huang, F. G. Ramos, G. Agnello, and V. P. LaBella, Phys. Rev. B **71**, 033302 (2005).
[16] M. Jamet, A. Barski, T. Devillers, V. Poydenot, R. Dujardin, P. Bayle-Guillemaud, J. Rothman, E. Bellet-Amalric, A. Marty, J. Cibert, R. Mattana, and S. Tatarenko, Nat. Mater. **5**, 653 (2006).
[17] J.-S. Kang, G. Kim, S. C. Wi, S. S. Lee, S. Choi, S. Cho, S. W. Han, K. H. Kim, H. J. Song, H. J. Shin, A. Sekiyama, S. Kasai, S. Suga, and B. I. Min, Phys. Rev. Lett. **94**, 147202 (2005).
[18] D. Bougeard, N. Sircar, S. Ahlers, V. Lang, G. Abstreiter, A. Trampert, J. M. LeBeau, S. Stemmer, D. W. Saxey, and A. Cerezo, Nano Lett. **9**, 3743 (2009).
[19] C. Awo-Affouda, M. Bolduc, M. B. Huang, F. Ramos, K. A. Dunn, B. Thiel, G. Agnello, and V. P. LaBella, J. Vac. Sci. Technol. A **24**, 1644 (2006).
[20] S. Zhou, K. Potzger, G. Zhang, A. Mucklich, F. Eichhorn, N. Schell, R. Grotzschel, B. Schmidt, W. Skorupa, M. Helm, J. Fassbender, and D. Geiger, Phys. Rev. B **75**, 085203 (2007).
[21] K. Tanaka, E. Maruyama, T. Shimada, and H. Okamoto, *Amorphous Silicon* (Wiley, New York, 1999).
[22] D. Haskel, J. W. Freeland, J. Cross, R. Winarski, M. Newville, and F. Hellman, Phys. Rev. B **67**, 115207 (2003).
[23] E. Helgren, F. Hellman, L. Zeng, N. Sinenian, R. Islam, and D. J. Smith, Phys. Rev. B **76**, 184440 (2007).
[24] G. Dalba, P. Fornasini, M. Grazioli, and F. Rocca, Phys. Rev. B **52**, 11034 (1995).
[25] G. Hertel, D. J. Bishop, E. G. Spencer, J. M. Rowell, and R. C. Dynes, Phys. Rev. Lett. **50**, 743 (1983).
[26] F. Hellman, M. Q. Tran, A. E. Gebala, E. M. Wilcox, and R. C. Dynes, Phys. Rev. Lett. **77**, 4652 (1996).
[27] F. Hellman, D. R. Queen, R. M. Potok, and B. L. Zink, Phys. Rev. Lett. **84**, 5411 (2000).
[28] P. A. Lee and T. V. Ramakrishnan, Rev. Mod. Phys. **57**, 287 (1985).

[29] E. Helgren, N. P. Armitage, and G. Grüner, Phys. Rev. Lett. **89**, 246601 (2002).
[30] E. Helgren, G. Grüner, M. R. Ciofalo, D. V. Baxter, and J. P. Carini, Phys. Rev. Lett. **87**, 116602 (2001).
[31] W. Teizer, F. Hellman, and R. C. Dynes, Int. J. Mod. Phys. B **17**, 3723 (2003).
[32] W. Teizer, F. Hellman, and R. C. Dynes, Solid State Commun. **114**, 81 (2000).
[33] S. von Molnar, A. Briggs, J. Flouquet, and G. Remenyi, Phys. Rev. Lett. **51**, 706 (1983).
[34] T. Dietl, Semicond. Sci. Technol. **17**, 377 (2002).
[35] K. Moorjani and J. M. D. Coey, *Magnetic glasses* (Elsevier, New York, 1984).
[36] R. M. Zallen, *Physics of Amorphous Solids* (Wiley, New York, 1983).
[37] L. Zeng, E. Helgren, M. Rahimi, F. Hellman, R. Islam, B. J. Wilkens, R. J. Culbertson, and David J. Smith, Phys. Rev. B **77**, 073306 (2008).
[38] L. Zeng, A. Huegel, E. Helgren, F. Hellman, C. Piamonteze, and E. Arenholz, Appl. Phys. Lett. **92**, 142503 (2008).
[39] I. Štich, R. Car, and M. Parrinello, Phys. Rev. B **44**, 11092 (1991).
[40] N. C. Cooper, C. M. Goringe, and D. R. McKenzie, Comput. Mater. Sci. **17**, 1 (2000).
[41] P. W. Anderson, Phys. Rev. **124**, 41 (1961).
[42] L. Zeng, E. Helgren, F. Hellman, R. Islam, and D. J. Smith, Phys. Rev. B **75**, 184404 (2007).
[43] J. A. Mydosh, *Spin Glasses: An Experimental Introduction* (Taylor & Francis, London, 1993).
[44] M. Liu and F. Hellman, Phys. Rev. B **67**, 054401 (2003).
[45] S. Picozzi, L. Ottaviano, M. Passacantando, G. Profeta, A. Continenza, F. Priolo, M. Kim, and A. J. Freeman, Appl. Phys. Lett. **86**, 062501 (2005).
[46] S. Picozzi, A. Continenza, and A. J. Freeman, Phys. Rev. B **70**, 235205 (2004).
[47] K. Laaziri, S. Kycia, S. Roorda, M. Chicoine, J. L. Robertson, J. Wang, and S. C. Moss, Phys. Rev. Lett. **82**, 3460 (1999).
[48] U. Gottlieb, A. Sulpice, B. Lambert-Andron, and O. Laborde, J. Alloys Compd. **361**, 13 (2003).
[49] R. Car and M. Parrinello, Phys. Rev. Lett. **60**, 204 (1988).
[50] M. Hortamani, L. Sandratskii, P. Kratzer, and I. Mertig, New J. Phys. **11**, 125009 (2009).
[51] H. Wu, P. Kratzer, and M. Scheffler, Phys. Rev. Lett. **98**, 117202 (2007).